J13.3 THE IMPACT OF THE MEAN CLIMATE ON ENSO SIMULATION AND PREDICTION

Xiaohua Pan*[1]
Bohua Huang [1, 2]
J. Shukla [1, 2]

1 Department of Atmospheric, Oceanic and Earth Sciences, College of Science,

George Mason University, Fairfax, VA

2 Center for Ocean-Land-Atmosphere Studies, Calverton, MD

1. Introduction

The El Niño/Southern Oscillation (ENSO) variability simulated by fully coupled global ocean-atmosphere general circulation models (CGCMs) has been assessed in numerous multimodel intercomparison projects (e.g., Neelin et al. 1992; Mechoso, 1995; Latif et al., 2001; AchutaRao and Sperber, 2002; Davey et al., 2002). More recently, several studies (Joseph et al. 2006; Leloup et al. 2008) also examined CGCMs' ENSO simulations under the forcing of the 20th century greenhouse gas. In both cases, it is found that some major ENSO characteristics are not well captured by most of these models. Temporally, the simulated ENSO cycle is more regular than the observed one and anomalous events occur too frequently in the models. Spatially, the sea surface temperature (SST) anomalies in the tropical Pacific extend too far westward and are too narrowly confined to the equatorial zone.

The potential causes of these model deficiencies in the simulation of ENSO could be the coarse model resolution and inadequate parameterizations of the sub-scale physical processes. Both factors not only can affect the simulated ENSO characters directly, they also cause deficiencies in the model mean climate and indirectly affect the model ENSO. ENSO is now well understood as an oscillation superimposed on a mean climate over the tropical Pacific (Bjerknes 1969). The mean climate can be defined as the long-term averaged mean climate of SST and surface wind stress in the tropical Pacific. Figure 1 shows the observed mean climate of SST and surface wind stress in the tropical Pacific. The mean SST features an east-west asymmetry near the equator, with cold water in the eastern and warm water in the western Pacific associated with easterly trade winds. A north-south asymmetry is also present in the eastern Pacific where warm water is located north of equator and cold water is present along the coast of Peru with cross-equatorial southerly trade winds straddling in between. The existence of these asymmetries is crucial for the formation of both the annual cycle (e.g., Xie 1994) and ENSO (Cane and Zebiak 1987).

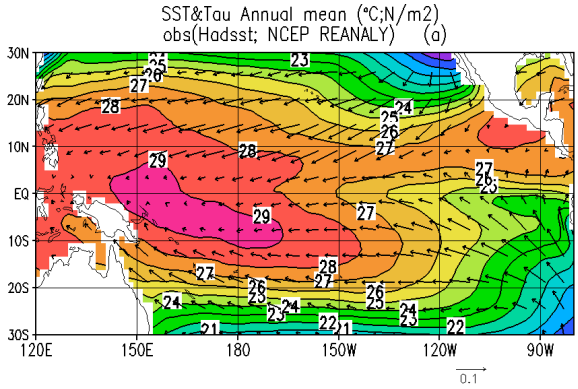

Figure 1. The spatial distributions of the annual mean SSTs (°C) and wind stress vector (N/m^2) over the tropical Pacific for Observation. The SST data is from Hadley center monthly mean SST for1900-1999; the wind stress vector is from NCEP reanalysis for1948-2003. The shading is SSTs, and the vector is windstress with the magnitude of 0.1 N/m^2

* *Corresponding author address*: Xiaohua Pan
4041 Powder Mill Road, Suite 302
Calverton, MD 20705-3106 USA
E-mail: xpan@cola.iges.org

However, the simulated mean climate has substantially weakened the asymmetric mean structure. For instance, cold SST bias in the central equatorial Pacific substantially reduces the temperature of the warm pool, while the warm bias near the coast of Peru weakens the meridional SST gradient. As a result, the mean SST field becomes more conducive for the occurrence of a robust "double ITCZ". These deficiencies in the simulated mean climate are likely responsible for some of the unrealistic ENSO properties in the coupled model (Li and Hogen 1999; Manganello and Huang 2008).

This study examines the impact of mean climate on the simulation, predictability and prediction of ENSO. Moreover, we demonstrate that the mean state also can strongly influences the annual cycle in the eastern equatorial Pacific. To achieve a more realistic model mean SST field, we have applied a heat flux correction to a state-of-the-art coupled model, the Community Climate System Model version 3 (CCSM3). It has been widely used in tropical climate research and demonstrated to suffer from both the mean state bias and errors in ENSO simulation (e.g., Deser et al., 2006) as we have described above. CCSM3 is considered as a member of the national multi-model ensemble for operational climate forecast. However, besides the work done by Kirtman and Min (2008), little is known about its ENSO prediction skill. This study provides more information on it.

2. Models

Community Climate System Model (CCSM) has been developed at NCAR and made available to the scientific community. Its third version (CCSM3) is released in June 2004 (Collins et al. 2006). It is comprised of four components: atmosphere, ocean, land and sea ice, which are coupled together through a flux coupler. This version also includes new updates of all component models. The atmosphere is Community Atmosphere Model Version 3 (CAM3), the land surface model is Land Surface Model version 3.0 (CLM3), the sea ice model is Sea Ice version 5.0 (CSIM5) and the ocean model is Parallel Ocean Program version 1.4.3 (POP). In this study, we use T85 resolution at CAM3, corresponding to a spatial resolution of 1.4°. It has 26 vertical levels. The spacing of the POP grids is 1.125° in the zonal direction and roughly 0.5° in the meridional direction with higher resolution near the equator. The vertical dimension is treated using a depth (z) coordinate with 40 levels extending to 5.37 km.

3. Experiment design

3a. Heat flux correction scheme

The primary goal of the present research is to study the impact of the mean climate on the simulation, predictability and prediction of ENSO variability rather than to correct the model bias. For this purpose, a sensitivity simulation is performed in which a simplified empirical scheme is applied by adjusting the surface heat flux into the ocean and the model results are compared with a control simulation. This method has been used in another coupled CGCM with satisfying results (Manganello and Huang 2008). Specifically, a time independent surface heat flux correction term (ΔQ) is added to the atmospheric surface heat flux before passing to the ocean. ΔQ is defined as,

$$\Delta Q = - \Delta SST \times R$$

where ΔSST is the100-year (1900-1999) mean state SST bias of the control run in comparison with observations. The adjustable coefficient R with unit W/m^2K converts the SST error to heat flux. ΔQ is constant in time and kept identical for both the simulation and all forecast experiments described in Sections 3b and 3c. The surface heat flux correction is applied at the air-sea interface by adding ΔQ into the surface trace flux terms (i.e., net surface heat flux excluding net solar radiation) in the ocean component model at the daily coupling frequency. Given SST changes of 1K, the heat flux changes approximately 15 W/m^2 in a fully coupled model (Doney et al. 1998). Considering the sharp warm biases along the coast of Peru (even beyond 4°K in some places), a moderate R with value of $10W/m^2$ per K is chosen in the tropical region between 30°S-30°N, where the interaction of air and sea is responsible for a strong relationship among anomalous SST, surface wind stress, convection and ocean heat content, and ENSO is a dominant phenomenon. This coefficient descends linearly to zero from 30°S to 40°S and 30°N to 40°N. The meaning of the heat flux correction is straightforward. It takes heat away from regions with the warm bias (e.g. off the coast of Peru) and put heat into regions with the cold bias (e.g., the central equatorial Pacific).

3b. Heat flux corrected simulation

The control and heat flux corrected simulations are hereafter referred to as the *contrl* and *flx* simulations, respectively. The *flx* simulation is integrated for 55 years from an initial state of the atmosphere and ocean derived from the *contrl* simulation. The model is spun up for five years and only the last 50 years of its output are

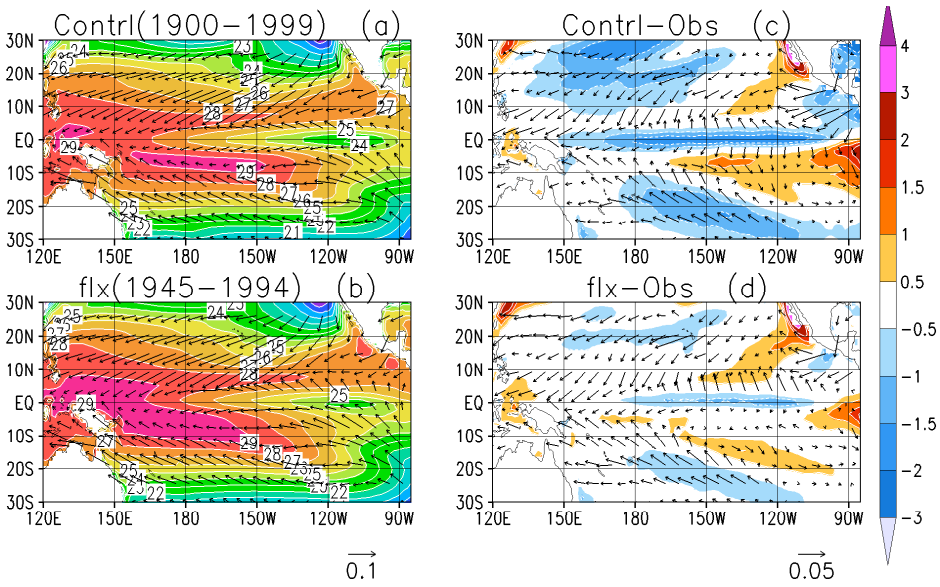

Figure 2. *Left panel:* The spatial distributions of the annual mean SSTs (°C) and wind stress vector (N/m^2) over the tropical Pacific for *contrl* and *flx*. *Right panel:* biases in *contrl* and *flx*. The observed SST data is from Hadley center monthly mean SST for1900-1999; the observed wind stress vector is from NCEP reanalysis for1948-2003; *contrl* is for 1900-1999; and *flx* is for 1945-1994. The shading is SSTs, and the vector is windstress with the magnitude of 0.1 N/m^2 in the left panel and 0.05 N/m^2 in the right panel.

used in our analysis. Since both the *flx* and *contrl* simulations are forced by observed 20th century greenhouse gases and volcanic forcing, the model years are labeled as calendar years with respect to its real-time greenhouse gas level.

3c. Heat flux corrected Prediction

In order to assess the impact of the mean climate on ENSO prediction and predictability, two sets of seasonal hindcast experiments are performed with and without the heat flux correction using CCSM3, denoted as the *flx* and *contrl* forecasts, respectively. Since the ENSO predictability is seasonally dependent, hindcasts are initialized on January 1st and July 1st in each year from 1982 to 1998. Each hindcast is integrated for 12 months. The initialization strategy follows that of Kirtman and Min (2008), using ocean initial conditions from analyses of the GFDL ocean data assimilation. The initial conditions for the atmosphere-land, and sea ice are derived from an AMIP-type run with prescribed real-time SST. For each oceanic initial condition, a 3-member ensemble hindcast is generated with perturbed conditions of the atmosphere, land and sea ice.

4. Results

4a. Mean climate

The simulated annual mean SST is remarkably improved in the *flx* experiment relative to the *contrl* (Figure 2b and d), due to the surface heat flux correction. The simulated equatorial cold bias is reduced by about 0.5°C, which extends less towards the Western Pacific. Meanwhile, the warm bias off the coast of South America is less pronounced with amplitude reduced by about 0.5 °C. Away from the equator, the cold bias also becomes less pronounced in *flx*.

The simulated annual mean wind stress is also improved in the *flx* experiment relative to the *contrl* (Figure 2b and d), especially in the eastern Pacific where the SST warm bias occurs. The southerly off the coast of the South American in *flx* is more similar to the observed both in amplitude and direction (Figure 2c). Even the cross-equatorial southerly wind, which is largely missing in *contrl*, is reproduced in *flx*. It should be pointed out that the improvement in the surface wind stress is a dynamical response to the changes in the SST because no empirical adjustment is exerted upon the surface wind or wind stress.

4b. Seasonal cycle

The seasonal cycle of equatorial SST from the observations and simulations is shown in Figure 3. The observed SST (left panel) exhibits a dominant annual cycle with the “cold tongue” weakest in March-April and peaking in August-October in the equatorial eastern Pacific. There is a pronounced westward propagation in the eastern and central equatorial Pacific. The *contrl*

experiment (middle panel) produces an unrealistic strong semi-annual cycle in the eastern Pacific instead, with the "cold tongue" decaying in April-May (one month later than observed) and peaking in July-August (one month earlier than observed), as well as the unrealistic secondary cooling in February and warming in November-December. Additionally, there is no obvious tendency of westward propagation. In contrast, *flx* (right panel) reproduces the observations reasonably well with a pronounced annual cycle and western propagation in the eastern Pacific. The artificial cold and warm centers in February and November-December in *contrl* is eliminated, although the coldest anomalies still appear too early, suggesting a too quick decay of the cold tongue. In *flx*, the enhanced annual cycle is generated dynamically because the heat flux correction employed in the coupled model is time independent and does not contribute to the annual oscillation directly.

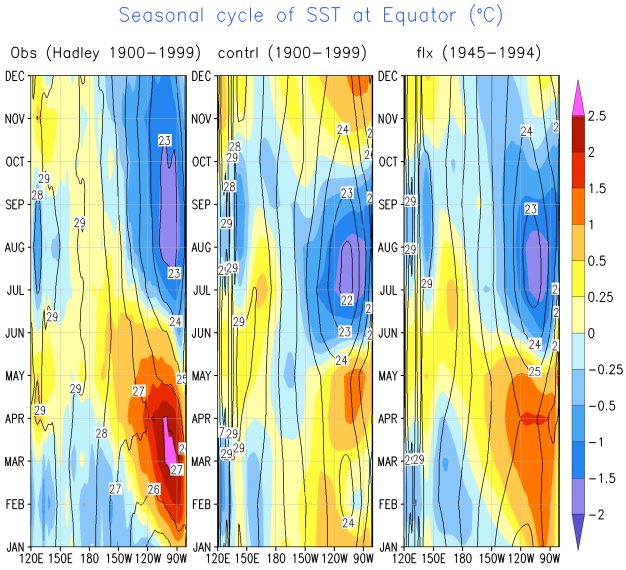

Figure 3. The seasonal cycle along the equatorial Pacific region (5°S-5°N) for SSTs (°C). The shadings represent the seasonal anomalies relative to the annual mean, while the contours represent the total value. The vertical axis indicates the month-of-year, varying from the bottom to top.

The seasonal cycle of the equatorial meridional wind stress is shown in Figure 4. Unlike its strong semi-annual SST fluctuation, *contrl* produces a strong annual cycle in its meridional wind stress (middle panel). A major unrealistic feature is the quite strong northerly winds of 2 m/s persisting from January to March, which cools down the sea surface through excessive evaporation and causes the artificial cold center of SST in Febuary (Middle panel, Figure 3). On the other hand, the *flx* (right panel) reproduces a well persistent cross-equatorial southerly throughout a year in the equatorial eastern Pacific (indicated by contours) although weaker than observed. The seasonal variation of this southerly in *flx* experiment is more similar to that in the observations (left panel) with weak southerly in the spring season, compared to the northerly in the *contrl* experiment.

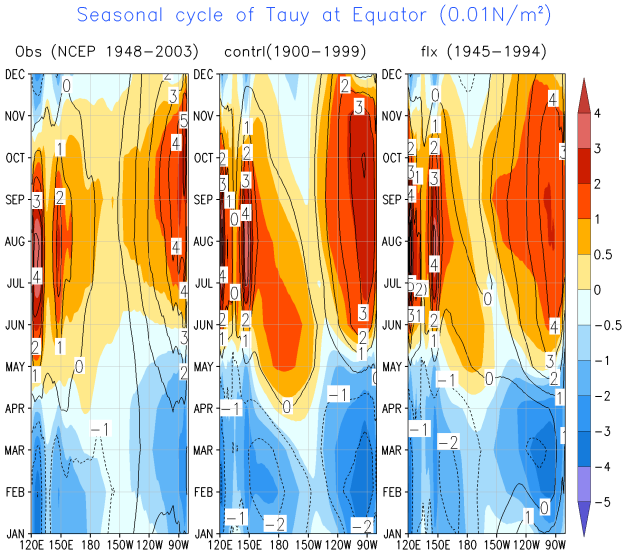

Figure 4. The seasonal cycle along the equatorial Pacific region (5°S-5°N) for Meridional wind stress (0.01N/m2). The shadings represent the seasonal anomalies relative to the annual mean, while the contours represent the total value. The vertical axis indicates the month-of-year, varying from the bottom to top.

This persistent cross-equatorial southerly meridional wind stress in the *flx* experiment significantly contributes to the realistic SST annual cycle in the eastern Pacific. Xie (1994) and Li and Philander (1996) revealed that this south-north asymmetric structure is important in determining the annual cycle. By constantly removing a given amount of heat from the sea surface near the South American coast as designed in the flux correction scheme, a larger air mass contrast is produced between the north and south of equator due to the change of the density of air above. The larger pressure gradient across the equator forces a cross-equatorial southerly. Both the evaporation and upwelling are correspondingly strengthened off the coast of South American, where the thermocline is shallow. Consequently, the SST is

reduced there, and the meridional SST gradient and thus the cross-equatorial southerly are reinforced. Although the heat flux correction is constantly applied at certain place, it can be balanced by the sensible, latent, and long-wave radiative surface heat fluxes, which are all responsive to the flux correction and induce changes of SST and surface wind. The ocean transport processes (e.g., advection and diffusion) also can adjust the heat balance. When a new equilibrium is reached, the south-north asymmetry in mean state is established in the eastern Pacific. In addition, there is a seasonal variation in the persistent cross-equatorial southerly wind, intense during the northern summer while relaxed during the southern summer. Through the evaporation, the "cold tongue" below develops in the northern summer and decays during the southern summer. Thus, an annual cycle of SST is present in the equatorial eastern Pacific.

4c. ENSO simulation

The power spectrum analysis on the Nino3.4 SST anomaly index reveals the dominant frequencies among the interannual variability and their corresponding amplitudes. The spectral density calculation is based on the Fourier method. Figure 5 presents the power spectrum of the 50-year Nino3.4 SST anomaly index with seasonal cycle removed for the observations and the two experiments. In the observations, a dominant 4-years period and a secondary dominant quasi-biennial period are indicated by the peaks of the spectral density. However, the *contrl* experiment exhibits a distinct and robust quasi-biennial oscillation, which is a major deficiency of CCSM3 (Deser et. al. 2006). In contrast, the biennial oscillation is absent in *flx* and

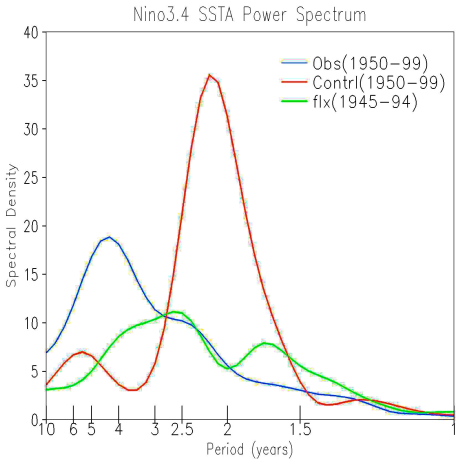

Figure 5. Power spectrum of 50-year Nino3.4 SST anomaly index. The observed SST data is from Hadley center monthly mean SST for1950-1999; **contrl** is for 1950-1999; and **flx10** is for 1945-1994.

replaced by a dominant period of 3 years and a secondary dominant period of 1.5 years in a broader spectral band, which is closer to the observations. The overall area under the spectral density curve in the *flx* experiment is much less than those from the observations and in *contrl*, indicating that the surface flux correction weakens the amplitude of the model interannual variability.

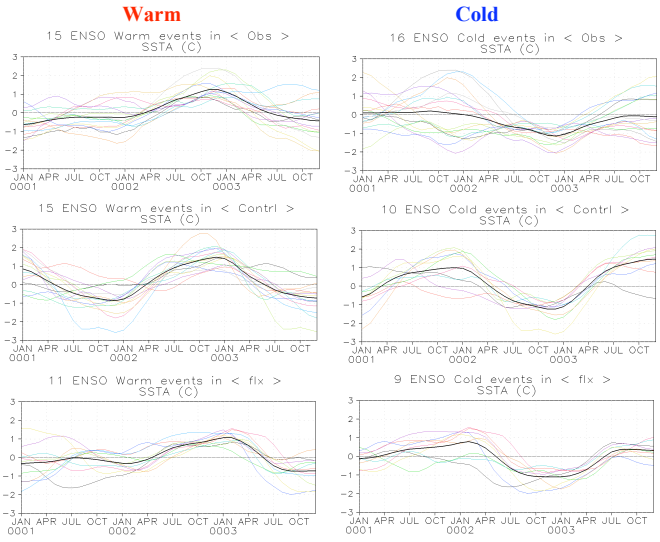

Figure 6. The evolution of composite ENSO events represented by the Nino3.4 SSTA. The colorful curves are individual cases and the black curve are the average of those individual cases.

The modification of the ENSO period is also reflected in the evolution of the composite ENSO event represented by the Nino3.4 SST anomalies in Figure 6. The thin curves with various colors refer to the individual events, chosen with the criteria that the averaged Nino3.4 SST anomaly indexes for five consecutive months from October to the February in the following year is greater than or equal to (less than) 3/4 (-3/4) standard deviation. The thick black curve is the average of all events or a composite ENSO cycle. It is clear that, taking the warm event for example, a warm event is immediately preceded by a cold event as a demonstration of the feature of biennial oscillation in the *contrl* experiment. In contrast, the evolution of the warm event in the heat flux corrected experiment more resembles the observed one, which is usually developed from a more neutral state in stead. Similar results are displayed in the composite cold events as shown in the right panel of Figure 6. As mentioned in section 4b, a stronger annual cycle is reproduced in the eastern Pacific due to the realistic south-north asymmetric structure. The

irregularity of ENSO is likely the result of the nonlinear interaction of this annual cycle with the interannual variability (Tziperman et al. 1994; Jin et al. 1994).

4d. ENSO prediction

The skill of forecasts is accessed by the anomaly correlation coefficient (ACC) and the root mean square error (RMSE) against the corresponding observations as shown in Figure 7. The ACC measures similarities in phase of the forecasts and observations and the RMSE measures the average magnitude of the error. Note that both forecast and the observations are anomalies deviated from their corresponding monthly climatology. It has been found empirically that the level ACC=60% corresponds to the limit where the forecast does not exhibit any significant synoptic skill, thus it is used for the minimum score of a useful prediction skill in this study.

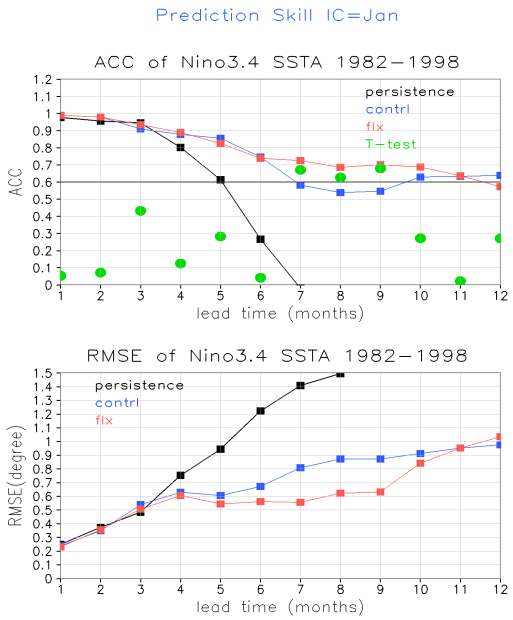

Figure7. Prediction skill measured by anomaly correlation coefficient (ACC) and root mean square error (RMSE) for January forecast using the Nino3.4 SSTA from 1982 to 1998. The skill of the persistence forecast is denoted by black curve, and the ensemble mean forecast flx10 is denoted by red curve and contrl by blue curve. In the panel of ACC, the green dot represents the standardized difference (ref. http://davidmlane.com/hyperstat/B8712.html) of the skill between forecast flx10 and contrl at each lead month. If the value is beyond 1.64, their difference is significant at the level 90% using student T test. The line ACC=0.6 denotes the criteria of a useful prediction skill.

Figure 7 gives the skill score for the January forecast as a function of the lead month. The skill score of a persistence forecast is taken as a reference for baseline skill. In general, skill scores of both the control and flux corrected forecasts drop steadily with respect to the leading month. During the first 4 months, the hindcasts may be influenced by the "spring barrier". They become more skillful than the persistence forecast beyond the first 3 months. At the first 6 months lead time, the skill scores for both the forecast *contrl* and *flx* are relative high (> 0.7) but largely indistinguishable from each other. At longer lead times of 7-9 months, the forecast *flx* has higher skill (around 0.7) than the forecast *contrl*. Its RMSE shows slower error growth during this period, consistent with the ACC. The forecast *contrl* and *flx* have comparable error in the first 6 months. The forecast *contrl* has larger errors of up to 0.3 °C at lead times of 7-9 months. However, their difference is not statistically significant at the 90% level as denoted by the green dots in ACC plot. Therefore, the robustness of improved prediction skill in the heat flux corrected hindcasts needs to be tested with more cases (17 years in the current study).

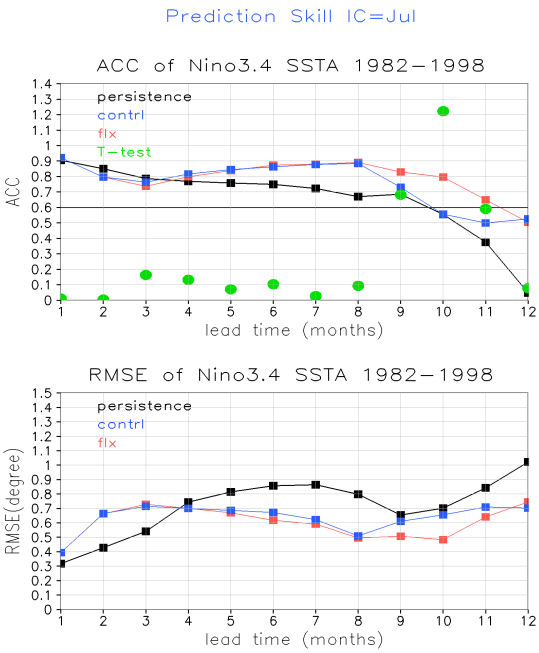

Figure 8. Same as Figure 7 but for July initial conditions.

The skill scores for the July forecasts are shown in Figure 8. The forecast *flx* has a skillful forecast up to 11 months, whereas the control forecasts are skillful for only the first 9 months. Both have similar skill in the first

8 months. After that time, the forecast skill drops rapidly in the forecast *contrl*, which might be related to the "spring barrier". At lead times of 9-11 months, the forecast *flx* has higher prediction skill than the forecast *contrl* with the higher ACC and lower RMSE, up to 0.2 and 0.2 °C respectively. However, their differences are again not statistically significant at 90% levels.

5. Summary

In this study we have investigated the impact of mean climate on the simulation, prediction and predictability of ENSO. A time-independent surface heat flux correction scheme is designed to modify the mean climate by correcting the mean climate biases in CCSM3. The main results are summarized below.

(1) The mean climate is improved in the heat flux corrected simulation with reduced warm biases off the coast of Peru and reproducing a persistent southerly in the eastern equatorial Pacific.

(2) A realistic annual cycle of SST in the eastern Pacific is generated in the heat flux corrected simulation because of the more realistic asymmetry in the mean climate there. Like CCSM3, Many GCMs have a difficulty to simulate a realistic annual cycle. Therefore, this study indicates that this problem might be resolved by improving the mean climate structure there.

(3) The ENSO behavior appears sensitive to the improvement of mean climate. An irregular cycle with longer period is simulated in the heat flux corrected run.

(4) This study indicates a slightly higher prediction skill of ENSO by improving the mean climate in the heat flux corrected hindcasts, although its robustness needs verification.

REFERENCES

AchutaRao, K. and K. Sperber, 2002: Simulation of the El Niño Southern Oscillation: results from the coupled model intercomparison project. Clim. Dyn., 19, 191-209.

Bjerknes, J., 1969: Atmospheric teleconnections from the equatorial Pacific. Mon. Wea. Rev., 97, 163–172. Cane MA, Zebiak SE, Dolan SC. 1986. Experimental forecasts of El Niño. Nature 321: 827–832.

Collins, W.D., C.M. Bitz, M.L. Blackmon, G.B. Bonan, C.S. Bretherton, J.A. Carton, P. Chang, S.C. Doney, J.J. Hack, T.B. Henderson, J.T. Kiehl, W.G. Large, D.S. McKenna, B.D. Santer, and R.D. Smith, 2006: The Community Climate System Model Version 3 (CCSM3). J. Climate, 19, 2122–2143.

Davey, M., M. Huddleston, K.R. Sperber et al., 2002: STOIC: A study of coupled model climatology and variability in tropical ocean regions, Clim. Dyn., 18, 403-420.

Deser, C., A. Capotondi, R. Saravanan, and A. Phillips, 2006: Tropical Pacific and Atlantic climate variability in CCSM3. J Climate, 19, 2451–2481.

Doney, S.C., W.G. Large, and F.O. Bryan, 1998: Surface Ocean Fluxes and Water-Mass Transformation Rates in the Coupled NCAR Climate System Model*. J. Climate, 11, 1420–1441.

Kirtman, B. P. and D. Min, 2008: Multi-Model Ensemble Prediction with CCSM and CFS. Mon. Wea. Rev. (in press).

Jin, F.-f., J. D. Neelin and M. Ghil, 1994: El Niño on the Devil's Staircase: Annual subharmonic steps to chaos, Science, 264, 70-72.

Joseph, R., and S. Nigam, 2006: ENSO Evolution and Teleconnections in IPCC's Twentieth-Century Climate Simulations: Realistic Representation? J. Climate, 19, 4360–4377.

Latif, M., K. Sperber, and co-authors, 2001: ENSIP: intercomparison project. Clim. Dyn., 18, 255-276.

Li, T., and S.G.H. Philander, 1996: On the annual cycle of the eastern equatorial Pacific. J. Climate, 9, 2986-2998.

Li, Tianming, Hogan, Timothy F, 1999: The Role of the Annual-Mean Climate on Seasonal and Interannual Variability of the Tropical Pacific in a Coupled GCM. J. Climate, 12,780-792

Manganello, Julia V.; Huang, Bohua, 2008: The influence of systematic errors in the Southeast Pacific on ENSO variability and prediction in a coupled GCM. Clim. Dyn., DOI:10.1007/s00382-008-0407-5.

Mechoso, CR, AW Robertson, and Co-authors 1995: The seasonal cycle over the tropical Pacific in general circulation models. Mon. Wea. Rev., 123, 2825-2838.

Neelin, J. D.; Latif, M.; Allaart, M. A. F.; Cane, M. A.; Cubasch, U.; Gates, W. L.; Gent, P. R.; Ghil, M.; Gordon, C.; Lau, N. C.; Mechoso, C. R.; Meehl, G. A.;

Oberhuber, J. M.; Philander, S. G. H.; Schopf, P. S.; Sperber, K. R.; Sterl, K. R.; Tokioka, T.; Tribbia, J.; Zebiak, S. E., 1992: Tropical air-sea interaction in general circulation models. Clim. Dyn., 7 (2) , 73-104.

Tziperman, E., L. Stone, M. A. Cane and H. Jarosh, 1994: El Niño Chaos: Overlapping of resonances between the seasonal cycle and the Pacific Ocean-Atmosphere oscillator. Science, 264, 72-74.

Weaver, A.J. and T.M.C Hughes, 1996: On the incompatibility of ocean and atmosphere models and the need for flux adjustments. Clim. Dyn., 12, 141-170.

Xie, S.P., 1994: On the Genesis of the Equatorial Annual Cycle. J. Climate, 7, 2008–2013.